

Simulation of reconstructions of the polar ZnO (0001) surfaces

H. Meskine, P. A. Mulheran

*Department of Process & Chemical Engineering, University Of Strathclyde,
James Weir Building, 75 Montrose, Glasgow G1 1XQ, United Kingdom*

Surface reconstructions on the polar ZnO(0001) surface are investigated using empirical potential models. Several possible reconstructions based around triangular motifs are investigated. The quenching of the dipole moment in the material dominates the energetics of the surface patterns so that no one particular size of surface triangular island or pit is strongly favoured. We employ Monte Carlo simulations to explore which patterns emerge from a high temperature quench and during deposition of additional ZnO monolayers. The simulations show that a range of triangular islands and pits evolve in competition with one another. The surface patterns we discover are qualitatively similar to those observed experimentally.

I. INTRODUCTION

Zinc oxide has a wide range of applicability from electronics to catalysis.¹ For example it is used as part of ZnO/Me/ZnO (Me=metal) multilayer functional glass coatings designed to filter heat-generating infra-red solar radiation. This is usually achieved by incorporating a thin low emissivity metal layer a few nanometres thick.² In the case where silver is used to construct a ZnO-Ag-ZnO sandwich, it has been shown^{3,4} that the lower Ag(111)/ZnO(0001) interface may fail for reasons not yet fully understood, leading to a sizable cost increase in the manufacturing of these devices. To understand this effect, one needs to characterise the interfacial structure that arises from the growth of Au on Zn(0001). A prerequisite for this is a fundamental understanding of the Zn(0001) surface that templates this growth.

Zinc oxide (zincite) has the well-known wurtzite structure with lattice parameters at room temperature and ambient pressure of $a = 3.25 \text{ \AA}$, $c = 5.207 \text{ \AA}$, and $u = 0.3825$, and space-group $P6_3mc$ (no. 186 in crystallographic tables).^{5,6} The structure may be understood as two interpenetrating hexagonal lattices, with each Zn (resp. O) sitting at the centre of a distorted O (resp. Zn) tetrahedron. The crystal when cut along the (0001) or (000 $\bar{1}$) planes is known to be a type III polar material according to the Tasker classification.⁷⁻⁹ That is to say that the unit cell is comprised of alternative negative and positive charged layers. This ultimately leads to a diverging electrostatic potential and should make the two polar surfaces of ZnO energetically unfavourable. This, however, is not the case as both the O-terminated and Zn-terminated polar surfaces show remarkable stability.¹⁰

Consider a slab of the material with bulk-terminated polar surface as used in typical computations (see Figure 1). Since the polar ZnO(0001) and ZnO(00 $\bar{1}$) surfaces occur naturally, there must be a mechanism to quench the dipole moment that exists normal to the slab surface. In order to quench this macroscopic dipole moment a transfer of charge across the slab of $(1 - 2u)\sigma \approx 0.235 \times \sigma$ is necessary, where σ is the surface charge density.¹⁰ This may be understood in terms of the electrostatic energy change when charge is moved from one surface to the

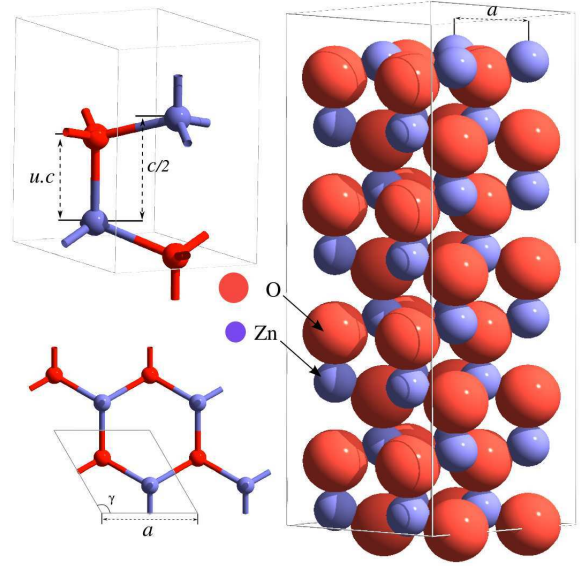


FIG. 1: Bulk crystal structure of wurtzite zinc-oxide with bulk lattice parameters $a = 3.25 \text{ \AA}$, $c = 5.207 \text{ \AA}$, and $u = 0.3825 \text{ \AA}$. In the bulk each ion is four-fold coordinated, while the surface atoms have only three-fold coordination. (colour online)

other in the direction of the internal electric field of the unreconstructed slab. Once sufficient charge has been moved, the counter electric field thus established cancels the one due to the bulk structure.

There are several mechanisms which may compensate the charge at the surface and counteract the macroscopic dipole moment of the semi-infinite crystal. Three, not necessarily incompatible, mechanisms have been considered in the literature: (i) adsorption of charged species e.g. hydroxilation, (ii) modification of the surface region by reconstruction, and (iii) direct charge transfer.

Until recently, the exact nature of such a mechanism in ZnO was not well understood, but recent theoretical and experimental studies¹¹⁻¹³ may have resolved the issue. A combination of surface microscopy techniques and Density Functional Theory (DFT) have indicated that, depending on the atmospheric environment, mechanisms

(i) and (ii) may be active in quenching the polarisation of the ZnO(0001) surfaces. For the Zn terminated orientation and in hydrogen-rich conditions, the surface is best passivated by adsorption of hydroxyl groups, while under low hydrogen partial pressure the surface tends to form triangular reconstructions that appropriately compensate the charge imbalance created by the surface cut. This work seems to rule out the third mechanism (iii) which had previously been proposed,¹⁴ involving charge transfer between O-terminated and Zn-terminated surfaces.

The above theoretical studies have relied on DFT which, while accurate, has a high computational cost and does not allow for a comprehensive search of the phase space. For example, in the case of the triangular reconstruction, STM scans show a range of triangle sizes while DFT studies only allow comparison of the energetics of single, relatively small configurations. In this work we present a study which combines fast, albeit less accurate, empirical potentials with Monte-Carlo simulations to study the structure and energetics of the polar ZnO(0001) surface, focusing on the surface reconstruction mechanism to quench the dipole. This approach is justified by the dominant role electrostatics plays in the surface reconstructions.¹³

The rest of the paper has the following structure. Section II describes the methodology employed, discussing the empirical potentials, surface relaxation calculations and Monte Carlo (MC) simulations. The results are presented in Section III, firstly for the energetics of various surface reconstructions, and then for the surface patterns that emerge from the MC simulations. The implications of the results are discussed in the following section, and our conclusions are given in the final Section V.

II. METHODOLOGY

A. Empirical potentials and surface slab calculations

Previous work by Catlow and coworkers^{8,15} has shown that empirical potentials are well suited to describe the details of the structure of the polar surfaces of most oxides. The parameters for a Buckingham potential are fitted following ref.¹⁶ to reproduce a variety of properties of Zinc Oxide. The potential was kept as simple as possible as is appropriate for the desired level of computation. For details of the validation of the interatomic potential parameters we refer the reader to ref.¹⁷. The total energy is computed by summing all pair interactions of the form

$$E(r_{ij}) = \frac{q_i q_j}{4\pi\epsilon_0 r_{ij}} + A \exp(-r_{ij}/\rho) - C/r_{ij}^6 \quad (1)$$

where $r_{ij} = \|\mathbf{r}_i - \mathbf{r}_j\|$ is the distance between two ions with charges q_i and q_j . In this work we use formal ionic charges $\pm 2e$ in all our computations. The first term of Eq. 1 is the long-range Coulomb pair interaction, while

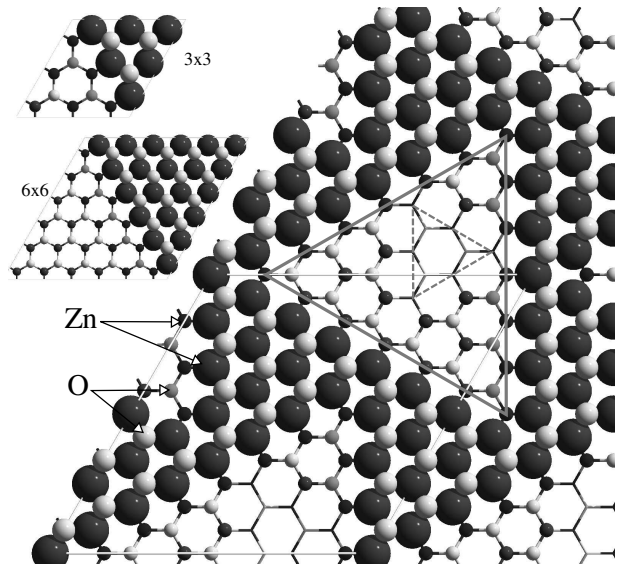


FIG. 2: Surface reconstruction $\sqrt{48} \times \sqrt{48}$ with a $n = 7$ triangular pit and an additional $m = 3$ inner pit within the larger triangle. The pits and terraces are created by removing Zn and O atoms. The topmost layer atoms are shown as large spheres (light red for O, dark blue for Zn) and the next layer atoms are shown by smaller spheres. The “bulk” atoms in the slab (everything below layer 2) are shown only by their bonds. Upper left we show the smaller triangular pits in a 3×3 and 6×6 surface unit cell.

the second and third terms correspond respectively to the repulsive and attractive terms of the short-range Buckingham pair potential.

The polarisability effects are described by a core-shell model, where the oxygen ion and its electronic cloud are modelled by a massive core and a mass-less shell carrying different charges (but with total charge $-2e$) and linked by a spring with energy

$$E^{\text{spring}} = \frac{1}{2} k_i \delta_i^2, \quad (2)$$

where k_i is the spring constant for ion i and δ_i is the core-shell distance. The empirical parameters A , ρ , C and k_i are determined by fitting to available experimental properties, such as the elastic constants. The fitting was performed with the GULP code¹⁸ using 8 potential parameters and various parameters from observable data. The computed bulk properties are compared to some relevant experimental values in Table I, and the values of the parameters used in this work are given in Table II.

Surface structure calculations were performed using three-dimensional periodic slabs with a large vacuum gap normal to the (0001) surface. Each slab contains one Zn-terminated surface and one O-terminated surface (see Fig. 1). Several reconstructions were created at the surfaces, where overall charge neutrality was ensured by removing the oppositely charged species from the other side of the slab. The outermost three surface layers on each side of the slab were allowed to relax. The energy

TABLE I: Comparison of some of the computed bulk properties to available experimental data. The experimental data are taken from standard tables¹⁹.

ZnO (wurtzite)	This work	Experiment
$a(\text{\AA})$	3.27	3.25
$c(\text{\AA})$	5.18	5.207
u	0.3819	0.3825
ε_{11}^T	4.22	9.26
ε_{33}^T	4.59	11.0
$C_{11}(\text{GPa})$	222.22	209.7
$C_{33}(\text{GPa})$	220.14	210.9

of different surface reconstructions were computed and an energy hierarchy constructed by comparing their surface energies. In order to estimate the surface energy of a given surface structure we use the total energy of the bulk unit cell as a reference state, in which case the surface energy is given by

$$\gamma = (E_{slab} - N_{cell} \times \varepsilon_{bulk}) / 2A \quad (3)$$

where $A = (N_s a)^2 \sin \gamma$ is the surface area of a slab (see Fig. 1) containing $N_s \times N_s \times N_z$ lattice units, E_{slab} is its relaxed total energy, and ε_{bulk} is the energy of a bulk unit cell. The quantity N_{cell} is the effective number of unit cells in the slab calculated by dividing the number of atoms in the slab by the number of atoms in a bulk unit cell (four in the case of ZnO). The factor of two accounts for the fact that the surface energy is the average surface energy of both sides of the slab.

It is important to emphasise again that the surface energy calculated in this way depends on slab thickness, unless we have perfect quenching of the dipole moment by creating a net charge transfer of $0.235 \times \sigma$ from one surface to the other in the reconstruction. For this reason, we will compare the energies of various surface structures using the same slab thickness $N_z = 6$ (twelve bilayers).

B. Monte-Carlo simulations

While a large number of structures may be explored using the above empirical model, it is impractical to find the lowest energy reconstruction using more and more elaborate guesses of the surface structure. In order to explore the large phase space of possible surface reconstructions we used Monte Carlo (MC) simulations with bulk lattice positions in a slab. The ions in the three upper-most bilayers of the slab are allowed to hop within their own bilayer and into the bilayers directly above or below. The simulations were started from different initial configurations and the system left to evolve according to the Metropolis algorithm. The initial configurations of the three uppermost bilayers were formed either by ion removals or by addition of ions to the clean slab. The overall charge neutrality was again ensured by adding/removing the oppositely charged species from the

TABLE II: Interatomic potential parameters used for the Buckingham potential. These were obtained by fitting to the experimental parameters of Tab. The spring Constants are in $\text{eV} \cdot \text{\AA}^{-2}$: $k_O = 15.52$, $k_{Zn} = 8.57$.

	$A(\text{eV})$	$\rho(\text{\AA})$	$C(\text{eV} \times \text{\AA}^6)$	r_{cutoff}
Zn-O ^s	499.6	0.359	0.0	0-10 \AA
O ^s -O ^s	22764.0	0.149	27.88	0-12 \AA

other side of the slab at the start of each simulation. As several studies⁷ have shown that the surface layer relaxation is less than 0.1\AA , for the sake of simplicity (and computational efficiency) we have neglected the effect of lattice relaxation on surface energy during these MC simulations.

A periodic slab model is used throughout, with $N_z = 6$ bulk unit cells along the c axis and a large vacuum of $L_z = 30 \text{\AA}$ added to form the super-cell. We verify that L_z is large enough by ensuring that the surface energy does not depend on L_z .

Successive configurations are generated by a series of nearest neighbour hops of either species selected at random at the uppermost Zn-terminated surface, with acceptance probability $e^{-\Delta E/k_B T}$ where T is the temperature and ΔE is the difference between total energies of the successive trial configurations. The bottom O-terminated surface reconstruction remains fixed in the simulations. The energy of a given atom in the slab is simply the sum of all its pair interaction with the other ions in the slab, with the pair interaction of ion i given by

$$\varepsilon_i = \sum_j E(r_{ij}). \quad (4)$$

Here, also for computational efficiency, we neglect the shell model component of the potential E^{spring} in the MC work only.

Since in this system we have no mechanism to quench any dipole across the slab, we ensure that the simulation is started from configurations with only a small residual dipole. The initial configuration of the MC simulation is then disordered by running the simulation at very high temperature leading to a fully disordered arrangement of the surface species, after which the temperature is lowered abruptly. The simulations are run at high temperature for a large enough number of steps that the initial ordering disappears.

The most expensive step of the simulation is the energy evaluation which includes long-range terms. The Coulomb sum being conditionally convergent in a periodic system, we make use of the Ewald sum²⁰⁻²²

$$E_R = \frac{1}{2} \sum_{\mathbf{n}}' \sum_{i,j} q_i q_j \frac{\text{erfc}(\alpha r_{ij,\mathbf{n}})}{r_{ij,\mathbf{n}}} \quad (5)$$

$$E_K = \frac{2\pi}{V} \sum_{\mathbf{k} \neq 0} \frac{e^{-k^2/4\alpha^2}}{k^2} |S(\mathbf{k})|^2 \quad (6)$$

TABLE III: Summary of the surface energies of several slabs, all with $N_z = 6$, and various total number of ions N . For the relaxed structures, the total energies are computed using GULP with the potential parameters listed in table II. The three outermost bilayers are allowed to relax while the rest of the slab is kept fixed. The vacancy concentration Θ_{vac} refers to the ratio of excess zinc *vacancies* in the uppermost surface layer created by removing zincs and oxygen from both sides of the slab.

	$\Theta_{vac}(ML)$	N	$\gamma(eV/\text{\AA}^2)$	
			rigid	relaxed
Bulk	-	-	-	-
2×2	0.500	88	4.210	4.162
4×4	0.250	352	0.255	0.086
$\sqrt{48} \times \sqrt{48}$	0.208	1034	0.306	0.245
6×6	0.055	856	2.248	1.447

$$E_0 = -\frac{\alpha}{\sqrt{\pi}} \sum_i q_i^2 + \frac{2\pi}{V} M_z^2 \quad (7)$$

where q_i is the formal charge of on i , \mathbf{r}_i is the position of the ion within the periodic slab, $S(\mathbf{k}) = \sum_i q_i e^{i\mathbf{k}\mathbf{r}_i}$ is the structure factor, and M_z is the z coordinate of the total dipole moment in the slab $\mathbf{M} = \sum_i q_i \mathbf{r}_i$. The parameter α is determined using the requirement that the Ewald sum is accurate yet efficient (see for example²³). It is worth noting that this expression is the more computationally efficient 3D version of the Ewald sum, not the two-dimensional version. If the vacuum slab is chosen large enough, only a correction due to the residual surface dipole is necessary.

The above total energy is computed once at the beginning of the run, and updated in the course of the simulation by only computing the energy difference between trial configurations. This considerably speeds up the computation of the energy and scales as $N^{1/2}$, where N is the number of particles in the system.

III. RESULTS

A. Surface reconstructions and energy hierarchy

On the zinc-terminated surface, it was experimentally shown that the triangular reconstructions are a single bilayer high. We therefore form the reconstructions by removing Zn and O atoms from the top-most bilayer and refer in what follows to the excess zinc vacancy concentration Θ_{vac} . Recall that we remove the opposite charge species from the O-terminated surface, keeping overall charge neutrality and imposing an electric field across the slab which compensates the bulk dipole moment for $\Theta_{vac} = 0.235$. The stability of the surface reconstruction is assessed by studying the surface energy as a function of this excess Zn vacancy concentration. Table III shows the surface energies for various zinc vacancy con-

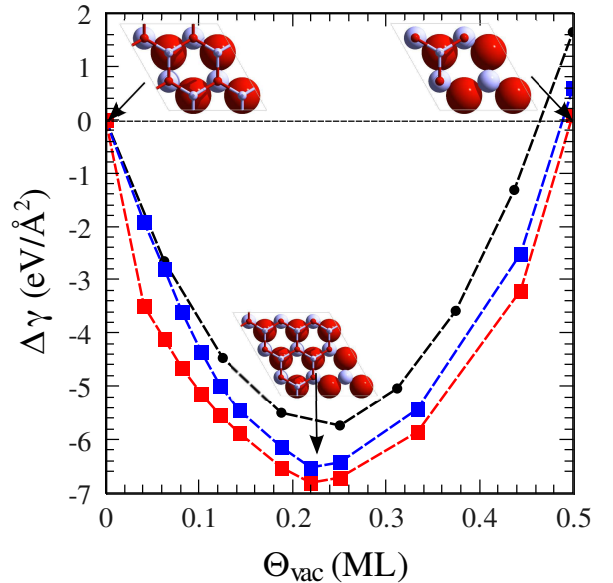


FIG. 3: Change in surface energy as a function of excess zinc vacancy on the surface expressed in fractions of a monolayer, where $\Delta\gamma = \gamma_{nvac} - \gamma_{clean}$ is the net surface energy compared to the surface energy of the bulk-terminated surface. The blue line refers to bulk position of the atoms while the red curve correspond to optimised position for the three bilayers nearest the surface. The surface energy change when creating *isolated* vacancies is shown by the black curve. Note that the small spheres refer to the topmost bilayer, while the larger ones refer to the bilayer immediately below it.

centrations and their corresponding surface reconstructions illustrated in Figure 2. Note that the reconstruction in the $\sqrt{48} \times \sqrt{48}$ surface unit cell as shown in Fig. 2 is not the most stable in this work, contrary to the prediction from density functional theory. This may be explained by a simple electrostatic argument, where the formal ionic representation of the species tends to overestimate the contribution of the Coulomb interaction, and thus favours smaller surface reconstructions.

We have computed the surface energies of several more surface reconstructions, for varying values of the excess zinc concentration, as well as for isolated vacancies. The results are summarised in Fig. 3 and are plotted in reference to the surface energy of the bulk-terminated slab with $N_z = 6$. We reiterate that the surface energy of the bulk-terminated slab is ill-defined due to the presence of a large surface dipole. It is only the *difference* in surface energies of various reconstructions that is of interest. The most stable reconstruction is the small 4×4 cluster with the smallest triangular vacancy (see Figure 2), with the more exotic reconstruction on the $\sqrt{48} \times \sqrt{48}$ surface cell lying nearby. The isolated vacancies consistently have a larger surface energy. Relaxation of the surface layers has a small effect on the surface stability, but does not impact the overall ordering of the various reconstruction energies.

In conclusion, the surface hierarchy obtained using the simple empirical potential shows no preference for large triangular reconstructions. Instead, small clusters which locally quench the surface dipole are preferred. The small impact of surface relaxation reflects the dominance of dipole moment quenching. This means that surface relaxation can be neglected in the MC simulations which follow, in which we allow the system to explore configuration space to see if larger reconstructions emerge naturally in our model with formal ionic charges.

B. Monte-Carlo Simulations

We have performed the MC simulation of a high temperature quench on a slab with $N_z = 6$, $N_s = 32$ and with the surfaces initially tessellated with the 4×4 triangular reconstructions giving $N = 22,528$ ions in total. Representative snapshots of the species distribution in the three uppermost layers of the Zn-terminated surface are shown in Fig. 4(a-c). We show the three uppermost bilayers separately (bilayer 1-3) at (a) the start of the simulation, (b) at the end of the high temperature run, and (c) after quenching. The figure clearly shows the effect of the high temperature, with the ordered triangular reconstructions completely disappearing from the first bilayer. The second and third bilayers are occupied as well, with no apparent ordering. After the system is cooled and left to evolve, large triangular reconstructions in the lowest bilayer begin to nucleate via aggregation of small triangular units. The smallest such unit is the one unit-cell triangle (three O ions surrounding one Zn ion) and is consistent with the earlier empirical potential result. The second bilayer only shows a few isolated a -side triangles, while the third layer is now completely empty. These observations are qualitatively identical for a large class of system size and parameters.

In Fig. 5 we show the evolution of the surface energy and the dipole moment normal to the surface in the simulation. During the high temperature anneal, both the surface energy and dipole moment are large in magnitude. This is due to the almost random placement of the surface layer ions into the 3 accessible bilayers, which leads to an obvious loss of bonding energy. The dipole moment also increases in magnitude since there is an excess of oxygen ions over zinc in the surface, so displacing them on average by one bilayer changes the total moment in the system. Upon quenching, the surface energy and dipole moment quickly reduce in magnitude, and in fact reach slightly lower values than in the starting configuration. At the start of the simulation, the dipole moment is $-162.29 \text{ e}\cdot\text{\AA}$, and is not zero since $\Theta_{vac} = 0.25$ rather than the ideal $\Theta_{vac} = 0.235$. After the temperature is raised, the dipole moment is roughly $-300 \text{ e}\cdot\text{\AA}$, since the topmost ions are now randomly distributed. By the end of the quench, after $N_{MC} = 4 \times 10^5$, its value is slightly lower, $-236.15 \text{ e}\cdot\text{\AA}$. This is achieved by the few ions occupying the second bilayer. For the surface energy, the

quenched value is $0.36 \text{ eV}/\text{\AA}^2$, as opposed to $0.59 \text{ eV}/\text{\AA}^2$ after heating.

The quenched MC simulation clearly shows that the system can evolve to a structure with preferred triangular motif and no regular tessellation of the surface. It is of interest to see if this effect also emerges during a simulation where the total number of ions in the surface layers increases over time, mimicking epitaxial growth. Starting from the end of a quenched simulation, we perform the MC annealing but now add pairs of $\text{Zn}^{2+}/\text{O}^{2-}$ ions at separate, randomly chosen sites in the three uppermost layers of the slab. Results from a simulation performed on a $N_z = 6$, $N_s = 32$ slab ($N = 8,800$) are shown in Fig. 6. Again, the simulation shows that triangular reconstructions form spontaneously, and grow larger by nucleation from characteristic smaller aggregates. We also see that the growth on the 2nd bilayer proceeds before the 1st bilayer is complete, leading to a surface with multiple ad-islands and pits of various size.

In Fig. 5 we also show how the surface energy and dipole moment change during the deposition simulation. The addition of the ions allows the system to find structures with decreasing magnitude of dipole moment, since thereby lowering the electrostatic energy. An interesting feature shown by Fig. 5 is that both surface energy and dipole moment oscillate as more ions are added, and reach even lower values as we deposit more and more ions. Thus the system finds a steady state with lower energy and dipole moment by making use of the larger number of degrees of freedom made available by the deposited ions.

IV. DISCUSSION AND CONCLUSION

It is observed from the STM results¹¹ that not one but several triangular features co-exist at the surface of Zn-terminated ZnO(0001). This behaviour also emerges in our Monte-Carlo simulations, for both the quenched structure in Fig. 4 and the deposition structure in Fig. 6. The reason for this can be traced to the small energy differences between the various surface reconstructions shown in Table III; there is no substantially preferred reconstruction, provided Θ_{vac} is close to 0.235 locally. Therefore the patterns that emerge in the MC simulations result from the competitive growth of energetically comparable triangular reconstructions. For this reason, we do not observe any long time coarsening of the structures in the simulation, as can be seen from the surface energy evolution shown in Fig. 5 during the quenched phase before deposition starts, and neither do we observe the system being restored to its regular tessellated starting configuration.

Our quenched MC simulation in Fig. 4 produces an interesting surface morphology that is reminiscent of the experimental STM images^{11,13}. Furthermore, the simulation with increasing surface coverage of Fig. 6 also includes other morphological features such as co-existing

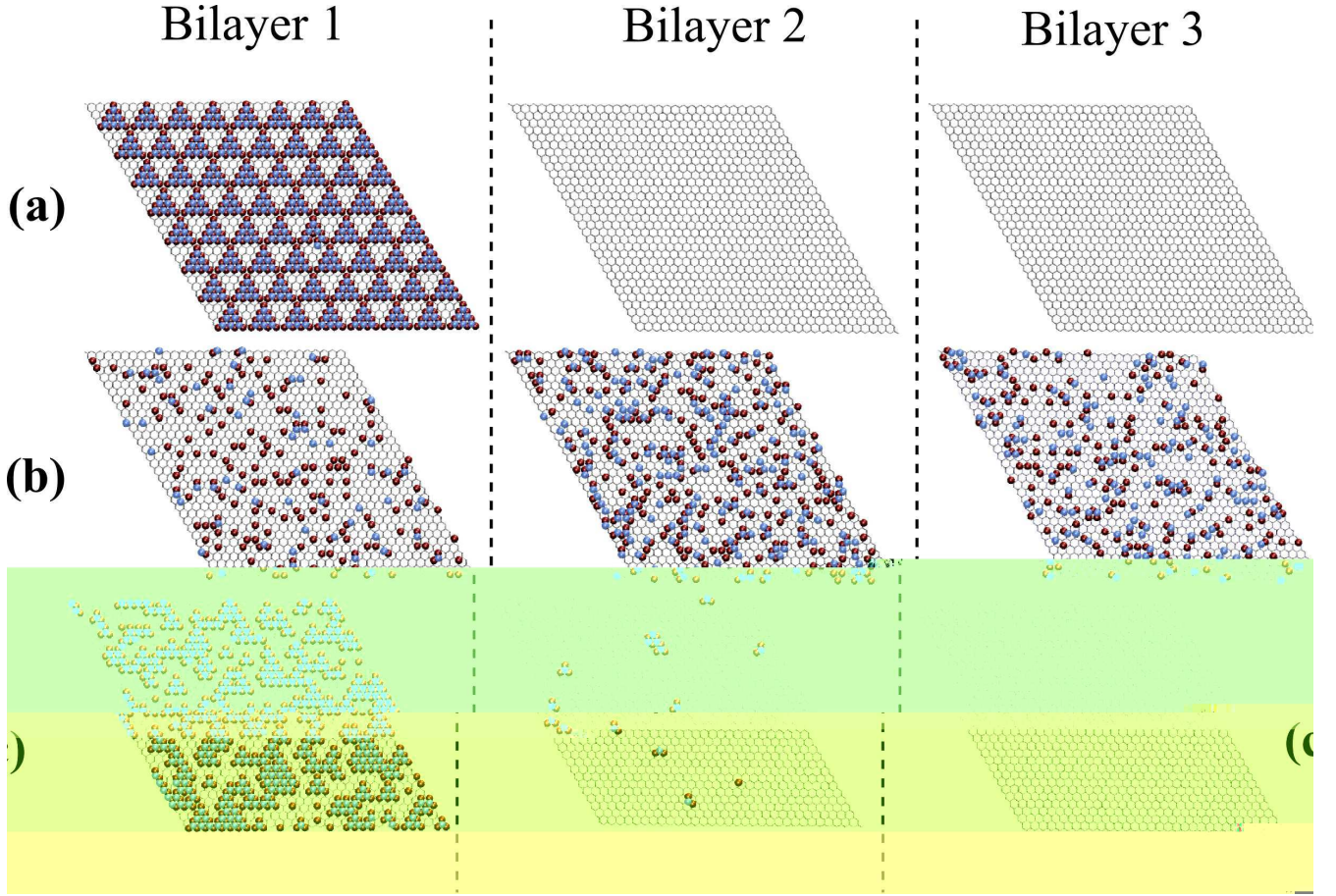


FIG. 4: Snapshot of Zn^{2+} and O^{2-} ions in the three topmost layers at different stages of the evolution of the MC simulation. The initial configuration (a) is evolved at high temperature until the initial reconstructions are melted giving rise to a random distribution of species in all three layers (b). The temperature is then abruptly at which point triangular structures begin to spontaneously in bilayer 1, while the top bilayers are gradually emptied.(c).

ad-islands and pits that are found experimentally. Therefore, we believe that the simulations capture some of the main physical processes that give rise to these surface reconstructions. However, it is important to note that the reconstructions found by the simulation are much smaller than those observed experimentally. The largest triangle observed from the MC simulation has a side of the order of 20\AA thus only reproducing the smallest clusters observed in the STM scans. It is possible that this is due to the lattice sizes and simulation durations that are accessible. Another explanation is that our use of formal charges ($\pm 2e$) on the ions is not justified in this system. Using formal charges probably overestimates the strength of the Coulomb interaction, thereby tending to make the triangular clusters at the surface more compact. Work to augment the current model using a charge

equilibration (or QEq) scheme²⁴ is therefore planned.

In conclusion, we believe that the models presented here do help to explain the Zn-terminated surface reconstructions observed experimentally. Whilst the accuracy of our models cannot compete with DFT, we are not restricted to studying individual reconstructions. The use of empirical potentials allows us to explore the phenomenology of the surface reconstructions more freely, and we find that a broad range of characteristic triangular motifs naturally emerge in our simulations, qualitatively consistent with the STM results.

Acknowledgement: This work was supported by the UK's Engineering and Physical Sciences Research Council grant EP/C524349 and by the University of Strathclyde.

¹ U. Ozgur et al., Journal of Applied Physics **98**, 041301 (2005).

² H. J. Glasser, *Large Area Glass Coating* (Von Ardenne Anlagentechnik, GmBH, 2000).

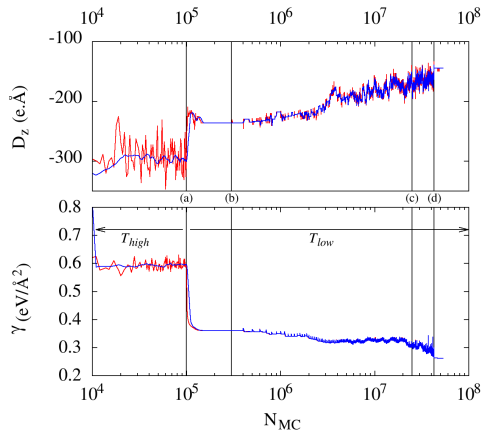


FIG. 5: Surface energy and dipole moment computed during a full Monte-Carlo run with $N_s = 32$. The simulation is started from a 4×4 tiled surface with a small residual surface dipole. We proceed to run the simulation at high temperature (T_{high}) for a large enough number of steps, then (a) quench to a lower temperature (T_{low}). The surface energy and dipole moment both settle at a lower value than initially. (b) Successive deposition of Zn/O pairs are then executed, up to 1 ML, then (c) 2 ML, allowing for a large enough number of steps between events to reach a new steady-state (d).

- ³ E. Barthel, O. Kerjan, P. Nael, and N. Nadaud, *Thin Solid Films* **473**, 272 (2005).
- ⁴ E. Ando and M. Miyazaki, *Thin Solid Films* **351**, 308 (1999).
- ⁵ S. C. Abrahams and J. L. Bernstein, *Acta Crystallographica Section B* **25**, 1233 (1969).
- ⁶ J. Albertsson, S. C. Abrahams, and Å. Kvik, *Acta Crys-*

- tallographica Section B* **45**, 34 (1989).
- ⁷ C. Noguera, *Journal of Physics: Condensed Matter* **12**, R367 (2000).
- ⁸ C. R. A. Catlow, S. A. French, A. A. Sokol, A. A. Al-Sunaidi, and S. M. Woodley, *Journal of Computational Chemistry* **29**, 2234 (2008).
- ⁹ P. W. Tasker, *Journal of Physics C: Solid State Physics* **12**, 4977 (1979).
- ¹⁰ J. Goniakowski, F. Finocchi, and C. Noguera, *Reports on Progress in Physics* **71**, 016501 (2008).
- ¹¹ O. Dulub, U. Diebold, and G. Kresse, *Physical Review Letters* **90**, 016102 (2003).
- ¹² O. Dulub, L. A. Boatner, and U. Diebold, *Surface Science* **519**, 201 (2002).
- ¹³ G. Kresse, O. Dulub, and U. Diebold, *Physical Review B* **68**, 245409 (2003).
- ¹⁴ A. Wander and N. M. Harrison, *The Journal of Chemical Physics* **115**, 2312 (2001).
- ¹⁵ L. Whitmore, A. A. Sokol, and C. R. A. Catlow, *Surface Science* **498**, 135 (2002).
- ¹⁶ D. J. Binks and R. W. Grimes, *Journal of the American Ceramic Society* **76**, 2370 (1993).
- ¹⁷ S. M. Woodley, *Database of published interatomic potential parameters*, <http://www.dfri.ucl.ac.uk/Potentials> (2009).
- ¹⁸ J. D. Gale, *Journal of the Chemical Society, Faraday Transactions* **93**, 629 (1997).
- ¹⁹ D. R. Lide, *CRC Handbook of Chemistry and Physics, 88th Edition* (CRC Press, 2007), ISBN 0849304881.
- ²⁰ I. Yeh and M. L. Berkowitz, *The Journal of Chemical Physics* **111**, 3155 (1999).
- ²¹ B. A., *Chemical Physics Letters* **400**, 62 (2004).
- ²² A. Bródka and A. A. Grzybowski, *The Journal of Chemical Physics* **117**, 8208 (2002).
- ²³ D. Fincham, *Molecular Simulation* **13**, 1 (1994).
- ²⁴ A. K. Rappe and W. A. Goddard, *The Journal of Physical Chemistry* **95**, 3358 (1991).

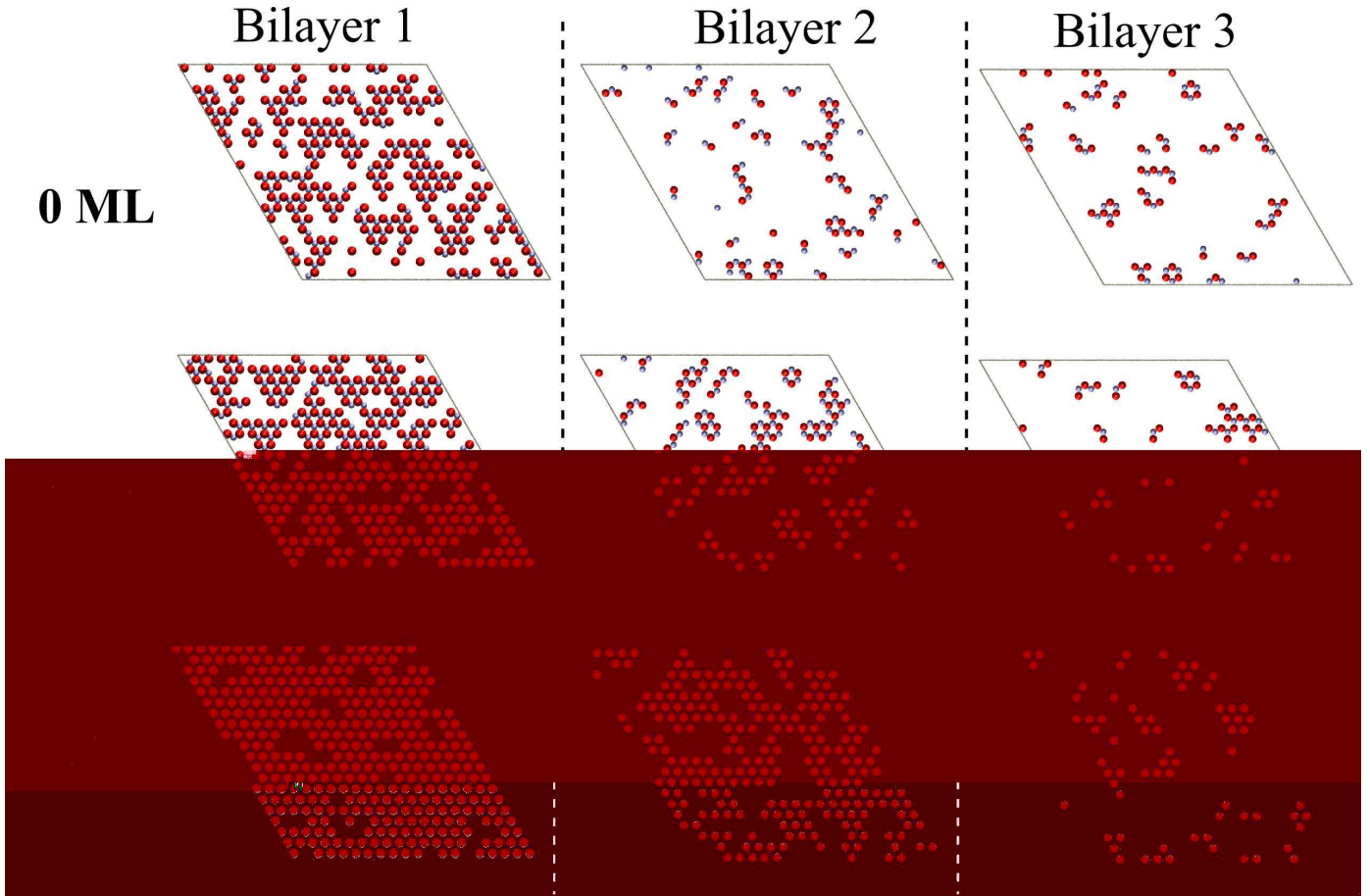


FIG. 6: In a way similar to 4 we show snapshots of the three upper bilayers as the deposition of a single monolayer (ML) is carried out. The top row shows the three bilayers before the deposition is started, the middle one after 0.5 ML was deposited, and the lower one after a full ML was deposited onto the surface. Note that the triangular features of the reconstruction are essentially conserved throughout the deposition.